PAPER

Check for updates

Growth and properties of spinel structure $Zn_{1.8}Co_{0.2}TiO_4$ single crystals by the optical floating zone method

Ying Liu,[ab] Dapeng Xu, [iD][a] Tian Cui, [iD][a] Huamin Yu,[ac] Xianfeng Li[a] and Liang Li [iD] *[a]

The spinel structure $Zn_{1.8}Co_{0.2}TiO_4$ single crystals with 5 mm diameter and 30 mm length were successfully grown by an optical floating zone method. The as-grown crystals were characterized by X-ray diffraction (XRD), Raman and X-ray photoelectron spectroscopy (XPS). Some Zn^{2+} ions at tetrahedral and octahedral sites should be replaced by doped transition metal Co^{2+} ions. The temperature-dependent Raman spectra of spinel $Zn_{1.8}Co_{0.2}TiO_4$ crystals were also described. The optical phonon behaviors of $Zn_{1.8}Co_{0.2}TiO_4$ are stable within the temperature range. The magnetic properties of $Zn_{1.8}Co_{0.2}TiO_4$ were investigated by using Physical Property Measurement System.

1. Introduction

The diluted magnetic semiconductors (DMSs) have attracted a great deal of attention.[1,2] As one of the most famous DMS materials, Co doped ZnO have been reported to possess ferromagnetic properties above room temperature.[3,4] Spinel type compounds, including normal (AB_2O_4) and inverse (A_2BO_4), have been intensively investigated for several decades because of their usefulness in many important technological applications and other branches of solid state sciences.[5,6] On the other hand, the inverse spinel structure Zn_2TiO_4 in cubic ($Fd\bar{3}m$) is a versatile host material, ideal for engineering optical and magnetic properties.[7] In addition, due to its excellent dielectric and photoelectrochemical properties, it is also applied in microwave devices.[8,9]

Doping with spin-unpaired 3d transition metals results both in a bandgap decrease and the appearance of magnetism.[10,11] Some studies have been conducted on the photoluminescence of Zn_2TiO_4 doped with transition metals and rare-earth ions, such as Cu^{2+}, V^{5+}, Cr^{3+} and Sn^{4+}. Up to now, there has been little research on the magnetism of Zn_2TiO_4 doped with Co^{2+} ions. However, the reported magnetic results of Co_2TiO_4 (ref. 12) and $ZnCoTiO_4$ (ref. 13) can be used as a key reference in the study of the magnetism of Zn_2TiO_4 doped Co^{2+}, because from another perspective, it can also be regarded as Co_2TiO_4 doped Zn^{2+}. The complex magnetic order of spinel Co_2TiO_4 indicates the existence of a quasi-long-range ferromagnetic state below T_N.[12]

It is well known that doped impurities and defects can affect the magnetic behavior of the materials.[14–16] Single crystals are more suitable for studying the intrinsic characteristics of materials. The optical floating zone technique is highly suited to the growth of high purity single crystals, especially metal oxides. Besides, based on the result of L. Mustafa[17] and G. D. Nipan,[18] we choose an optimization doping content (10%). Therefore, the aims of this work are the growth of $Zn_{1.8}Co_{0.2}TiO_4$ single crystals by optical floating zone method and investigations of the effects of Co dopant on the system and magnetic properties of $Zn_{1.8}Co_{0.2}TiO_4$ for the first time.

2. Experimental

Polycrystalline sample of $Zn_{1.8}Co_{0.2}TiO_4$ was obtained by the solid-state reaction technique. High purity (99.99% pure) ZnO, TiO_2 and Co_2O_3 powders were weighed and mixed. Then the powders were grounded with ethanol in an agate ball-milling machine to obtain a homogeneous mixture and heated in air at 1473 K for 20 h with intermediate grinding. The pretreated mixtures were reground and packed into a cylindrical shape rubber tube. Then they were hydrostatically pressed up to 70 MPa in a cold isostatic press, forming a cylindrical rod. Finally, the rods were sintered at 1500 K for 10 h in air, using as the feed and seed rods.

The crystals growth of $Zn_{1.8}Co_{0.2}TiO_4$ were carried out by the infrared-heating floating-zone furnace (Crystal Systems Inc. Model: FZ-T-10000-H-VP-VI, Japan) using 1000 W ×4 halogen lamps in four mirror as heating sources. The crystals were cut along their crystals axis directions and finely polished.

The X-ray diffraction (XRD) measurements were taken on a Rigaku D-max-r A 12 kW X-ray diffractometer using a Cu Kα

[a]State Key Laboratory of Superhard Materials, College of Physics, Jilin University, Changchun 130000, PR China. E-mail: lliang@jlu.edu.cn; Fax: +86 431 85167046; Tel: +86 431 85167955

[b]Changchun Institute of Technology, Changchun 130012, PR China

[c]Aviation University Air Force, Changchun 130022, PR China

radiation source. Structural refinements using the Rietveld method[19] were carried out *via* MAUD software. To determine the orientation of the crystals, a Bruker D8 Discover AXS with GADDS XRD[2] was employed. The Raman spectra (RS) were recorded by a Jobin-Yvon LABRAM-HR800 high resolution Raman spectroscope with λ_{ex} = 514.5 nm. The chemical properties of crystals were analyzed by X-ray photoelectron spectroscopy (XPS), which is an ESCALAB 250 electron energy spectrometer with Mg Kα (12 530.6 eV) as the X-ray excitation source. The magnetic susceptibility χ *versus* temperature T and magnetization M *versus* magnetic field H measurements were performed by using Physical Property Measurement System (Quantum Design, model: PPMS-16).

3. Results and discussion

In order to obtain a more stable crystal growth environment and reduce the generation of gas bubbles in the molten zone, crystals were grown in the air atmosphere and the seed and feed rods were rotated in opposite directions at the same rate of 6 rpm. The growth rate was 10 mm h^{-1}. The air flow of 0.1 L min^{-1} and the pressure of 0.1 MPa were applied. Moreover, a stable melting zone is very important to obtain a high-quality single crystal, which sometime dependent on the surface tension. And the surface tension of the melting zone dependent on the intrinsic properties, dopants and temperature of materials. In our case, due to the doped Co^{2+} ions affect the surface tension of the melting zone, the heating power needs to be reduced during the growth of Zn$_{1.8}$Co$_{0.2}$TiO$_4$ crystals to keep the stable of the melting zone.

The powder X-ray diffraction patterns of Zn$_{1.8}$Co$_{0.2}$TiO$_4$ single crystal are shown in Fig. 1a. The pattern can be identified as the spinel Zn$_2$TiO$_4$ structure (JCPDF no. 25-1164), which indicates that Co doping does not disturb the structure of Zn$_2$TiO$_4$. No additional peaks, such as CoO, Co$_3$O$_4$ or CoTiO$_3$ are observed indicating that no impurity exists in the Zn$_{1.8}$Co$_{0.2}$TiO$_4$ single crystal. The XRD results

are analyzed by the Rietveld method using the MAUD program[20] and sig = 1.21. The lattice parameter: space group is $Fd\bar{3}m$, $a = b = c = 8.4660$ Å, which is smaller than the pure Zn$_2$TiO$_4$ (8.48 Å).[21] Fig. 1b displays the XRD[2] pattern of the thin slice cut perpendicular to the growth direction and the photograph of as-grown Zn$_{1.8}$Co$_{0.2}$TiO$_4$ single crystal which is crack-free and black cylindrical rods with 5 mm in diameter and 30 mm in length. There is only one strong peak appears at $2\theta = 70.37°$, belonging to (620) plane. It indicates that the as-grown crystal is a single crystal with parallel to the (620) direction.

The chemical states of each element are crucial to study the properties of Zn$_{1.8}$Co$_{0.2}$TiO$_4$ crystal, especially the magnetic properties. In order to clarify the components and chemical states of elements of the Zn$_{1.8}$Co$_{0.2}$TiO$_4$ single crystals, XPS was performed and the XPS of Zn-2p, Ti-2p, Co-2p and O-1s were obtained, as shown in Fig. 2. For the XPS spectrum of Zn-2p, two main peaks assigned to Zn-2p$_{3/2}$ and Zn-2p$_{1/2}$ can be observed at 1021.7 and 1044.8 eV (Fig. 2a), respectively, which were ascribed to Zn^{2+}. Fig. 2b presents the Ti-2p XPS spectrum of the sample. The binding energy at 458.6 and 464.4 eV corresponded to Ti-2p$_{3/2}$ and Ti-2p$_{1/2}$, respectively.[22] It was noticed that only Ti^{4+} species and no Ti^{3+} species were observed in the Zn$_{1.8}$Co$_{0.2}$TiO$_4$ single crystal.

The Co-2p XPS spectrum of the sample is presented in Fig. 2c. It shows four peaks: a doublet and its corresponding shake-up satellites at slightly higher energies. The binding energies of 782.4 and 798.3 eV were obtained for Co-2p$_{3/2}$ and Co-2p$_{1/2}$, respectively. The energy difference of 15.9 eV between these two binding energy values for cobalt characteristic of Co^{2+} only, and no additional signatures for the Co^{3+} state (ΔE = 15.0 eV) and metallic Co.[23–25] Hence, we concluded that Co in our sample was 2+ state.

The XPS spectrum of O-1s was recorded and fitted into two peaks displayed in Fig. 2d. The peak at the low binding energy (530.1 eV) was assigned to the oxygen in the spinel lattice and the peak at the high binding energy (532 eV) was ascribed to the
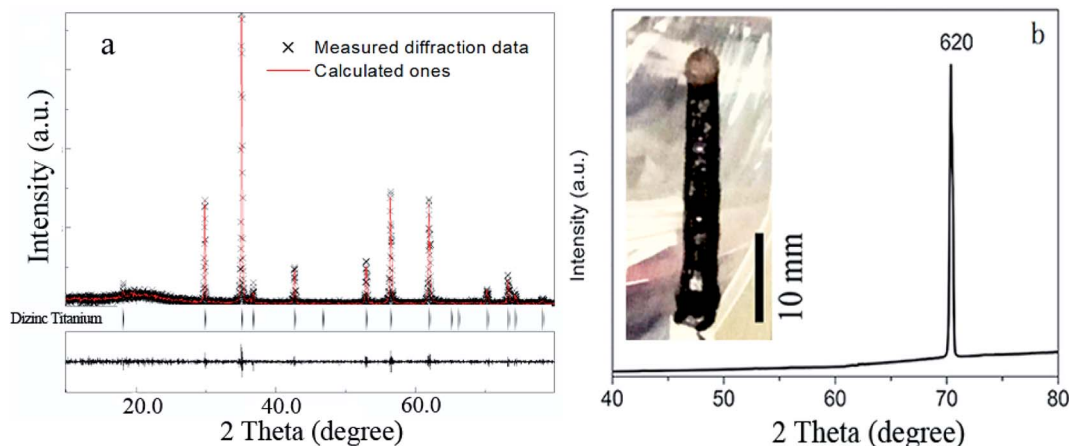

Fig. 1 (a) Rietveld refined XRD of Zn$_{1.8}$Co$_{0.2}$TiO$_4$ powder. The bottom line shows the difference profile between measured and calculated patterns. (b) XRD[2] pattern tested along the growth direction, the insert shows photograph of as-grown Zn$_{1.8}$Co$_{0.2}$TiO$_4$ single crystal in an infrared-heating furnace.
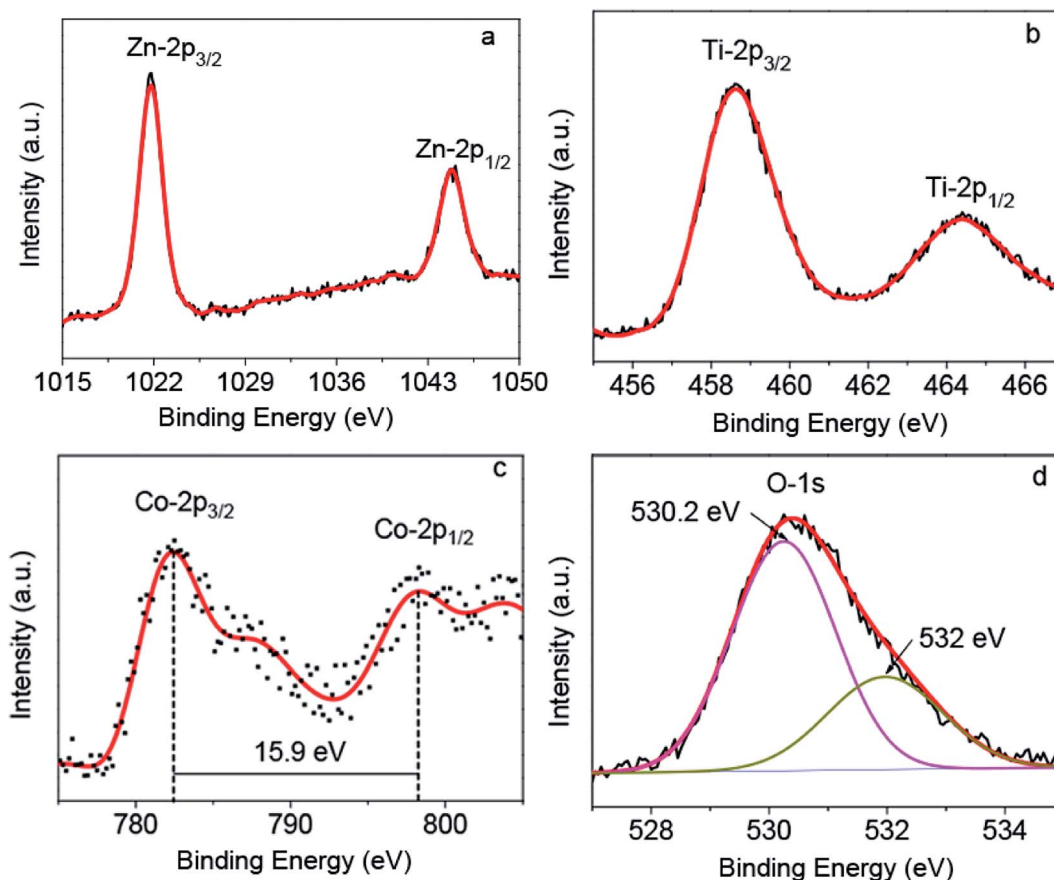
Fig. 2 (a) Zn-2p, (b) Ti-2p, (c) Co-2p and (d) O-1s XPS of $Zn_{1.8}Co_{0.2}TiO_4$ single crystal powder.

surface OH groups.[26] There is a small peak at 531.3 eV, which should be attributed to the general characteristic peak of oxygen defects, indicating that there were some oxygen defects in the grown $Zn_{1.8}Co_{0.2}TiO_4$ crystal.

Fig. 3 gives the Raman spectra for the as-grown $Zn_{1.8}Co_{0.2}$-TiO_4 crystals at room temperature. It can be seen that the Raman modes of 259 (F_{2g}), 306 (F_{2g}), 481 (E_g) and 724 cm^{-1} (A_{1g}) appear. The observed Raman spectra agree well with those of
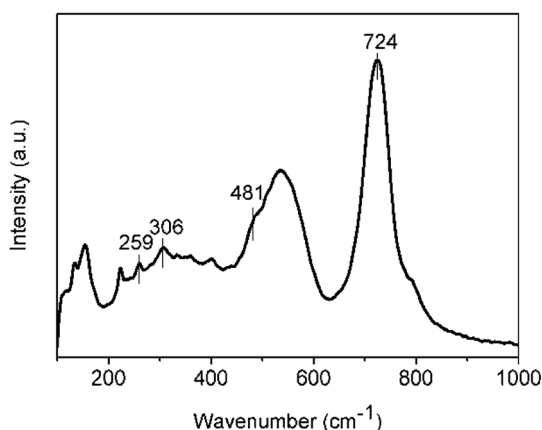
spinel Zn_2TiO_4.[17] The difference is that there is a lack of Raman peak representing F_{2g} mode at 348 cm^{-1}, and the weak Raman peak at 481 cm^{-1} has superimposed with the wide and strong peak at 535 cm^{-1} behind it. The modes, located at 154 and 535 cm^{-1}, do not belong to the Raman-active modes of spinel $Zn_{1.8}Co_{0.2}TiO_4$. The mode at 535 cm^{-1} was assigned to an order-disorder effect. The peak of 535 cm^{-1} in Zn_2TiO_4 is weaker than almost all other Raman peaks. However, it becomes the second strongest peak in the as-grown $Zn_{1.8}Co_{0.2}TiO_4$ crystal. Thereby, the order-disorder effect becomes stronger due to the doped Co^{2+}.

The Zn_2TiO_4 is an inverse spinel, and structure formula can be written as ($Zn(TiZn)O_4$), with a space group of $Fd\bar{3}m$ and typically described by a 56-atom unit cell. In this unit cell, 32 oxygen atoms comprise a face-centered cubic lattice with associated interstitial octahedral (O) and tetrahedral (T) sites. These T-sites are occupied by half of the divalent Zn cations, while O-sites are randomly filled with a stoichiometric mixture of divalent Zn and tetravalent Ti cations. While the doping Co^{2+} occupied T-sites and O-sites. And then the O-sites are occupied by three kinds of ions, including Co^{2+}, Zn^{2+} and Ti^{4+}. The structure is more complicated and the disorder effect of the O-sites becomes stronger. Therefore, the order-disorder effect significant enhanced by the doping of Co^{2+} and the bond at 535 cm^{-1} become very strong. On the other hands, the full

Fig. 3 The room-temperature Raman spectra for as-grown $Zn_{1.8}$-$Co_{0.2}TiO_4$ crystals.

width at half maximum (FWHM) of the A_{1g} mode at 724 cm^{-1} is 51 cm^{-1}, which is 11 cm^{-1} more than the pure Zn_2TiO_4 crystals, in which the FWHM of the A_{1g} mode is 40 cm^{-1}.[22] The FWHM can give the information about uniform of the bonds. The Co^{2+} ions replace the Zn at the T-sites and disturb the Zn–O tetrahedral should be the main reason for the boarder of the A_{1g} mode at 724 cm^{-1}. The Raman spectra can indicate that the as-grown $Zn_{1.8}Co_{0.2}TiO_4$ crystals are still spinel structure, and Co^{2+} ions replace part of Zn^{2+} ions, making the ions occupy randomly in tetrahedral and octahedral sites, resulting in enhancement of order-disorder effect.

To investigate temperature effects on the spinel structure of $Zn_{1.8}Co_{0.2}TiO_4$, the temperature-dependent Raman spectra were measured. A total of 18 temperature-measuring points were employed from 93 to 773 K at 40 K intervals. The Raman spectra obtained at each point are shown in Fig. 4a. The temperature-dependent Raman wavenumber of the 259 (F_{2g}), 306 (F_{2g}), 481 (E_g) and 724 cm^{-1} (A_{1g}) four peaks and FWHM of the A_{1g} mode were obtained, as shown in Fig. 5a and b, respectively. With the temperature increasing from 93 to 773 K, the common features are: (1) all the Raman peaks shifted towards the low wavenumber direction, (2) the peaks were broadened, (3) the intensity gradually decreased, (4) peaks with relative low intensity at low temperature disappear. Moreover, the vibration mode of 481 cm^{-1} (E_g) becomes fuzzier because the widths were too wide to be recognized when the temperature increases and superimposed with the peak of 535 cm^{-1}.

The A_{1g} mode located at 724 cm^{-1} corresponds to the local lattice effect in the tetrahedral (T) sublattice, while the modes at 306 and 481 cm^{-1} reflect local lattice effects in the octahedral (O) sublattice.[27] The relative intensity reflects the relative content of the corresponding mode compared with other modes. For undoped Zn_2TiO_4, when the temperature rising from 87 to 873 K, the intensity of A_{1g} mode at 724 cm^{-1}

becomes the second strongest and the Raman bands from O-site become the strongest.[22] The change of the relative Raman intensities of T and O sites indicates that the dislocation of Zn^{2+} cations from the T site to the O site, while Ti^{4+} cations may migrate from the O site to the T site.[22] In contrast, relative Raman intensities of T and O sites did not change after the Co^{2+} ions were doped in Zn_2TiO_4, as shown in Fig. 4b. The Raman intensity of A_{1g} mode, as the strongest bond, is significantly higher than the others during the whole temperature range. Therefore, the doping of Co^{2+} ions impeded the migration of Zn^{2+} and Ti^{4+} cations between O and T sites. Furthermore, no new Raman peak is observable, indicating that the spinel structure of $Zn_{1.8}Co_{0.2}TiO_4$ is stability at temperatures ranging from 93 to 773 K.

The magnetic properties of $Zn_{1.8}Co_{0.2}TiO_4$ single crystal powder are investigated. The temperature dependence of magnetic susceptibility (χ) under zero field cooling (ZFC) and field cooling (FC) conditions were measured at an external magnetic field of 500 Oe from 300 to 3 K as illustrated in Fig. 6. The two curves are superimposable exactly and increased as the temperature decreases. No separation of ZFC and FC was observed, indicating that there is no a glassy spin magnetic moment. The magnetic susceptibility (χ) is composed of two parts, which can be written as:

$$\chi(T) = C/(T - T_0) + \chi_{PP}$$

where the former represents a temperature dependent Curie–Weiss paramagnetism, χ_{PP} represents Pauli paramagnetism independent of temperature, C is the Curie–Weiss constant and T_0 is the Curie–Weiss temperature that provides information on the nature of magnetic exchange interactions in the system.[28,29] The positive T_0 characterizes ferromagnetic interactions while negative T_0 characterizes antiferromagnetic interactions. Further, temperature dependence of inverse magnetic susceptibility is shown in the insert of Fig. 6. The Curie–Weiss
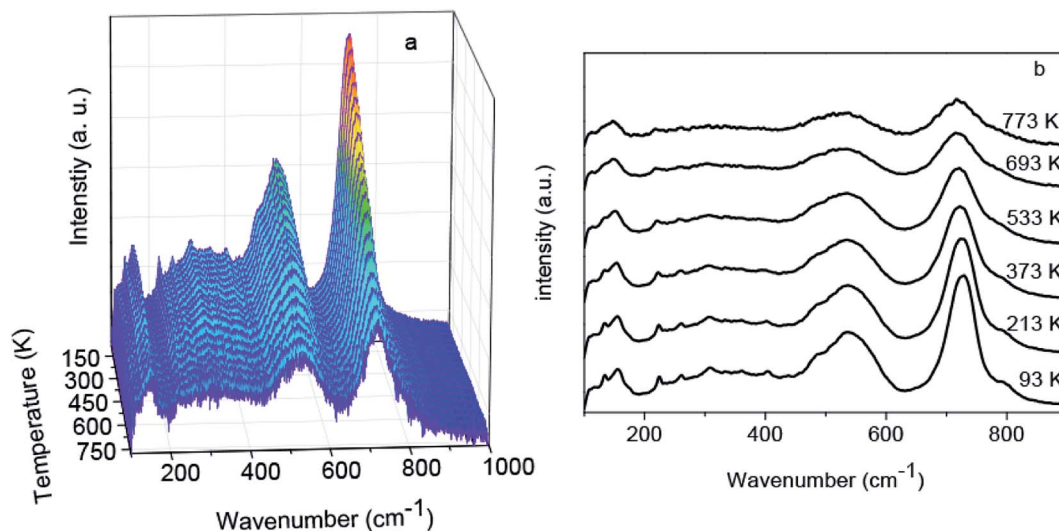

Fig. 4 (a) Full temperature-dependent Raman spectra of the $Zn_{1.8}Co_{0.2}TiO_4$ crystal in the range from 93 to 773 K. (b) Selected temperature-dependent Raman spectra.
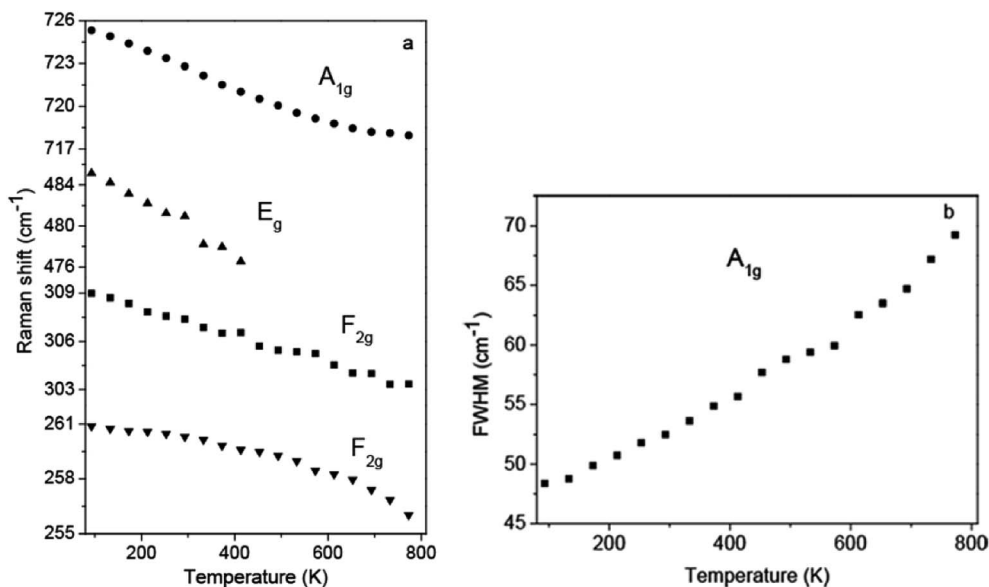
Fig. 5 (a) Temperature-dependent Raman shift for the selected Raman bonds. (b) Linewidth of A_{1g} modes as a function of temperature.
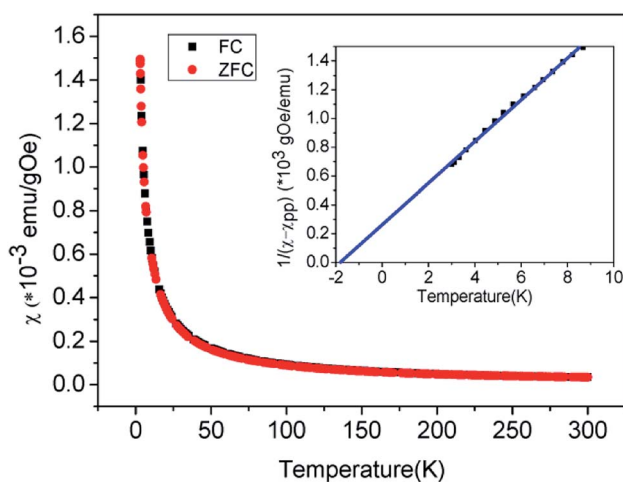

Fig. 6 Temperature dependence of magnetic susceptibility for $Zn_{1.8}Co_{0.2}TiO_4$ single crystal powder. The insert shows that temperature trend of the inverse Curie–Weiss susceptibility, with a linear fit to the data (a straight line).

temperature $T_0 = -1.8$ K, and negative value indicates the existence of a weak antiferromagnetic interactions. The observed antiferromagnetism is consistent with those reported for Co_2TiO_4 and $ZnCoTiO_4$,[12,13] but no spin glassy states have been found. The effective magnetic moment obtained from the Curie–Weiss constant ($C = 1.822$ emu K Oe^{-1} mol^{-1}) is 2.70 μ_B/Co.

The isothermal magnetization measurements were carried out in a magnetic field that varied between -30 and 30 kOe at different temperatures (300, 60, 20 and 5 K), as shown in Fig. 7. The magnetizations increase linearly at 300, 60 and 20 K, exhibiting an obvious paramagnetic behavior. This indicates that the sample has not underwent a transition from

paramagnetism to antiferromagnetism at the temperature of 20 K. As the temperature decreased to 5 K, the curve exhibits a little hysteresis, which indicates that a weak ferromagnetism is superposed on the antiferromagnetic curve. Furthermore, no saturation of the magnetization is observed below 30 kOe, due to the fact that the antiferromagnetic interactions not completely overcome in 30 kOe field. The existence of ferromagnetic state below T_N was observed to be the same as that of Co_2TiO_4 compound.[12] Ferromagnetism comes from the different Co^{2+} cations located in tetrahedral or octahedral sites, since the octahedral coordination requires orbital contributions, which are not present in the tetrahedral coordination. In other words, the ferromagnetism found also indicates that doped Co^{2+} ions take the place of some Zn^{2+} ions in tetrahedral and octahedral sites.
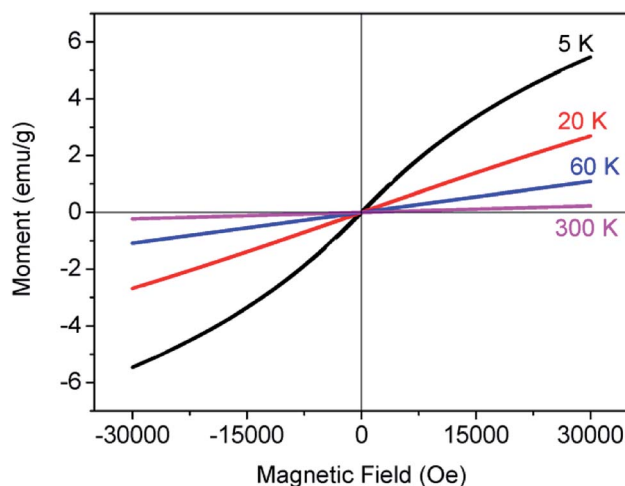

Fig. 7 M–H curves at different temperatures for $Zn_{1.8}Co_{0.2}TiO_4$ single crystal powder.

4. Conclusions

In summary, the $Zn_{1.8}Co_{0.2}TiO_4$ single crystals were grown by optical floating zone method. The XRD, Raman and XPS results indicated that Co^{2+} ions are replaced some Zn^{2+} at T and O sites. The temperature-dependent Raman spectra of spinel $Zn_{1.8}$-$Co_{0.2}TiO_4$ crystal were also described. The result shows that the optical phonon behaves of $Zn_{1.8}Co_{0.2}TiO_4$ is stable in the temperature range and doped Co^{2+} ions impeded the migration of Zn^{2+} and Ti^{4+} cations between octahedral and tetrahedral sites. The temperature dependence of magnetic susceptibility and the magnetization as a function of the applied magnetic field were performed, indicating that when the temperature up to 5 K, the sample underwent paramagnetism to antiferromagnetism transition. The effective magnetic moment is 2.70 μ_B/Co.

Conflicts of interest

There is no conflicts of interest regarding the publication of this paper.

Acknowledgements

References

1 H. Ohno, D. Chiba, F. Matsukura, T. Omiya, E. Abe, T. Dietl, Y. Ohno and K. Ohtani, *Nature*, 2000, **408**, 944.

2 R. Flederling, M. Keim, G. Reuscher, W. Ossau, G. Schmidt, A. Waag and L. W. Molenkamp, *Nature*, 1999, **402**, 787.

3 M. Venkatesan, C. B. Fitzgerald, J. G. Lunney and J. M. D. Coey, *Phys. Rev. Lett.*, 2004, **93**, 177206.

4 M. H. F. Sluiter, Y. Kawazoe, P. Sharma, A. Inoue, A. R. Raju and U. V. Waghmare, *Phys. Rev. Lett.*, 2005, **94**, 187204.

5 H. Martinho, N. O. Moreno, J. A. Sanjurjo, C. Rettori, A. J. Garcia-Adeva, D. L. Huber, S. B. Oseroff, W. Ratcliff, S. W. Cheong, P. G. Pagliuso, J. L. Sarrao and G. B. Martins, *Phys. Rev. B: Condens. Matter Mater. Phys.*, 2001, **64**, 024408.

6 B. N. Kim, K. Hiraga, K. Morita and Y. Sakka, *Nature*, 2001, **413**, 288.

7 Y. Inaguna, A. Aimi, Y. Shirako, D. Sakurai, D. Mori, H. Kojizani, M. Akaogi and M. Nakayama, *J. Am. Chem. Soc.*, 2014, **136**, 2748.

8 Y. Yang, R. Scholz, H. J. Fan, D. Hesse, U. Gosele and M. Zacharias, *ACS Nano*, 2009, **3**, 555.

9 L. Li, F. Li, T. Cui, Q. Zhou and D. Xu, *Phys. Status Solidi A*, 2012, **209**, 12.

10 D. Shoemaker and R. Seshadri, *Phys. Rev. B: Condens. Matter Mater. Phys.*, 2010, **82**, 214107.

11 J. Ruiz-Fuertes, T. Bernert, M. He, B. Winkler, V. L. Vinograd and V. Milman, *Appl. Phys. Lett.*, 2014, **105**, 071911.

12 S. Nayak, S. Thota, D. C. Joshi, M. Krautz, A. Waske, A. Behler, J. Eckert, T. Sarkar, M. S. Andersson, R. Mathieu, *et al.*, *Phys. Rev. B: Condens. Matter Mater. Phys.*, 2015, **92**, 214434.

13 D. Ruiz-Leóna, F. Mompeanb, J. Prado-Gonjalb, F. M. José, G.-H. Mar and R. Schmidt, *J. Eur. Ceram. Soc.*, 2018, **38**, 4986.

14 M. Li, J. Li, L.-Q. Chen, B.-L. Gu and W. Duan, *Phys. Rev. B: Condens. Matter Mater. Phys.*, 2015, **92**, 115435.

15 G. S. Chang, J. Forrest, E. Z. Kurmaev, A. N. Morozovska, M. D. Glinchuk, J. A. McLeod, A. Moewes, T. P. Surkova and N. H. Hong, *Phys. Rev. B: Condens. Matter Mater. Phys.*, 2012, **85**, 165319.

16 R. Murugan, G. Vijayaprasath, T. Mahalingam and G. Ravi, *Ceram. Int.*, 2016, **42**, 11724.

17 L. Mustafa, S. Anjum, S. Waseem, H. Khurshid and S. Javed, *Mater. Today: Proc.*, 2015, **2**, 5638–5644.

18 G. D. Nipan, A. I. Stognij and V. A. Ketsko, Oxide ferromagnetic semiconductors: coatings and films, *Russ. Chem. Rev.*, 2012, **81**, 458.

19 H. Rietveld, A profile refinement method for nuclear and magnetic structures, *J. Appl. Crystallogr.*, 1969, **2**, 65–71.

20 L. Lutterotti, S. Matthies, H.-R. Wenk, A. S. Schultz and J. W. Richardson Jr, Combined texture and structure analysis of deformed limestone from time-of-flight neutron diffraction spectra, *J. Appl. Phys.*, 1997, **81**, 594–600.

21 R. B. Rankin, A. Campos, H. Tian, R. Siriwardane, A. Roy, J. J. Spivey, D. S. Sholl and J. K. Johnson, Characterization of bulk structure in zinc orthotitanate: A Density Functional Theory and EXAFS Investigation, *J. Am. Ceram. Soc.*, 2008, **91**, 584–590.

22 L. Li, S. H. Gao, T. Cui, B. X. Li, Q. Zhou, H. M. Yuan and D. P. Xu, *RSC Adv.*, 2017, **7**, 35477.

23 J. K. Kwak, K. H. Park, D. Y. Yun, D. U. Lee, T. W. Kim, D. I. Son, J. H. Han and J. Y. Lee, *J. Korean Phys. Soc.*, 2010, **57**, 1803.

24 J. G. Kim, D. L. Pugmire, D. Bhattagila and M. A. Langell, *Appl. Surf. Sci.*, 2000, **165**, 70.

25 S. C. Petitto, E. M. Marsh, G. A. Carson and M. A. Langell, *J. Mol. Catal. A: Chem.*, 2008, **281**, 49.

26 A. C. Tavares, M. I. da Silva Pereira, M. H. Mendonca, M. R. Nunes, F. M. Costa and C. M. Sá, *J. Electroanal. Chem.*, 1998, **449**, 91.

27 M. Mączka, M. Ptak, M. Kurnatowska and J. Hanuza, *Mater. Chem. Phys.*, 2013, **138**, 682.

28 M. H. Pegah, E. Panaitescu, D. Heiman, L. Menon and L. H. Lewis, *J. Mater. Res.*, 2013, **28**, 10.

29 X. Che, L. Li and G. Li, *Appl. Phys. Lett.*, 2016, **108**, 143102.